Pergamon

Int. J. Solids Structures Vol. 34, No. 30, pp. 4005–4018, 1997

0020-7683/97 $17.00 + .00

PII: S0020-7683(97)00001-2

ELASTIC-PLASTIC ANALYSIS OF A TRIANGULAR PYRAMIDAL INDENTATION

YUKITAKA MURAKAMI
Department of Mechanical Science and Engineering, Faculty of Engineering,
Kyushu University, Hakozaki, Fukuoka 812, Japan

and

MASAYA ITOKAZU
Department of Mechanical Engineering, Faculty of Engineering, University of the Ryukyus,
Senbaru 1, Nishihara Okinawa 903-01, Japan

(*Received* 18 *July* 1995; *in revised form* 15 *November* 1996)

Abstract—A particular formulation of the three-dimensional finite-element method is established for the elastic-plastic analysis of a triangular pyramidal indentation. Indentations on 0.46% carbon steel and 70/30 brass are analyzed by the proposed method using the tensile stress-strain curve for each material. The calculated results are in good agreement with the experimental results. The curve of the calculated load-penetration depth is analyzed with relation to the geometrical similarity and the mechanical properties. The extension of the plastic zone induced by the indentation made by an indenter is investigated using the analysis. © 1997 Elsevier Science Ltd.

1. INTRODUCTION

Magnetic hard disks are widely used for computer information storage systems, and research continues to increase the density of the information storage (Kaneko, 1991). The structure of the magnetic hard disk is composed of several thin layers with thickness ranging from a few to a few hundred nanometers. The information is stored in the magnetic layer of a disk which is covered with two protection layers. One protects the information from the contact of the head (slider), the electronic device for reading and writing the information on the magnetic layer, and another is a lubricant between the head and the protection layer. Decreasing the thickness of the protection layer to increase the density of information storage has been a major research goal. For strength evaluations, the mechanical properties of the protection layers must be determined. Recently, the ultra-low load hardness test has been considered as a useful tool for estimating the mechanical properties of a very small scale region or of a very thin layer and several hardness testers have been developed and applied to practical use (Pethica *et al.*, 1983; Doerner and Nix, 1986; Yanagisawa and Motomura, 1987; Tsukamoto *et al.*, 1987; Inamura and Suzuki, 1990; Yanagisawa, 1991; Ohmae and Tagawa, 1992; Shimamoto *et al.*, 1993).

The mechanical properties of the materials are estimated from the relationship between load and penetration depth measured by the ultra-low load hardness tester in which a triangular pyramidal diamond is used as the indenter. The advantage of using a triangular pyramidal diamond is that it is easier to prepare the tip with a sharp point as compared with four-faced pyramidal indenters which often have a chisel edge and conical indenters which cannot avoid a rounded tip; this is illustrated schematically in Fig. 1. While experimental studies using the ultra-low load hardness testers to determine the mechanical properties of materials have been conducted, there are few analytical investigations on the triangular pyramidal indentation. No theoretical solution for the problem of a triangular pyramidal indentation has yet been developed. For elastic materials, Barber and Billings (1990) and Bilodeau (1992) presented an approximate solution for triangular pyramidal

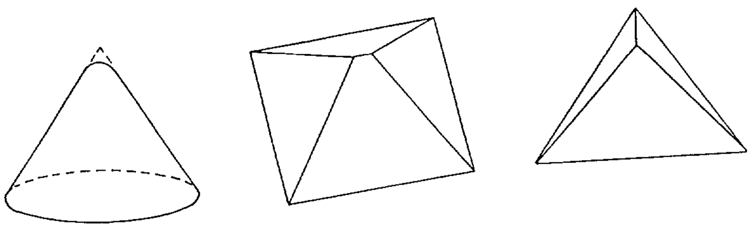

(a) Conical indenter (b) Square pyramidal indenter (c) Triangular pyramidal indenter

Fig. 1. Shape of indenter.

indentation. Olaf and Scheer (1993) carried out the simulation of the depth-sensing (triangular pyramidal) indentation process by a commercial FEM program using two dimensional as well as three dimensional models of the indenter and the specimen. They pointed out that the most important system parameters of depth-sensing indentation test are the geometry and the blunting of the indenter tip. The coupling of the influence of system and specimen parameters can only be separated using the combination of numerical and experimental investigations. Recently, Larsson *et al.* (1996) analyzed the Berkovich indentation test numerically, using a commercial FEM program, and experimentally, both on nano- and microscale. The Berkovich is the triangular pyramidal indenter whose total area of three surfaces is equal to that of four surfaces of the Vickers at the same height (Berkovich, 1951). They derived the universal formulae for hardness and total indentation load from the numerical results showing good agreement with experimental findings. Moreover they also checked the accuracy of relevant formulae for determining the elastic stiffness at initial unloading and concluded that the formulae are reliable regardless of the plastic hardening, at least for the range of moderate hardening investigated in their study.

The authors formulated a three-dimensional finite-element method for the elastic analysis of triangular pyramidal indentation in a previous paper (Murakami *et al.*, 1994). The calculated results of the FEM analysis clarified the influences of material elastic constants (Young's modulus and Poisson's ratio) and of the apical angle of triangular pyramidal indenters on the relationship between elastic load and penetration depth. Although the elastic FEM analysis can be applied to certain materials such as Corning glass and sapphire, in which the relationship between load and penetration depth behaves elastically below the threshold load (Page *et al.*, 1992; Shimamoto *et al.*, 1993; Murakami *et al.*, 1994), for most materials plastic deformation occurs under a small indentation load and the elastic analysis will not be valid.

In this paper, the method of elastic analysis for triangular pyramidal indentation (Murakami *et al.*, 1994) is extended to the elastic-plastic analysis which is based on the strain incremental plastic theory of Prandtl-Reuss equation. The method of the present paper enables one to analyze accurately the triangular pyramidal indentation without using commercial FEM programs. In order to verify the validity and accuracy, the proposed method is applied to a triangular pyramidal indentation at the micro-hardness region (maximum load is 9.8 N) on 0.46% carbon steel and 70/30 brass using the tensile stress-strain curve. The calculated results are compared with experimental results of micro-hardness tests using the triangular pyramidal diamond indenter. The curve of the calculated load-penetration depth is analyzed with relation to the geometrical similarity and the mechanical properties. Since there is no established method to evaluate the mechanical properties of materials with nano-meter size, the combined analytical-experimental method will be necessary. The promising method to solve the complicated problem of this kind must be proved its validity by the test of micro-mechanics level. Thus, we expect the availability of the present method as a possible analytical method to evaluate the mechanical properties in the ultra-low load hardness test.

2. ANALYTICAL METHOD

The three-dimensional FEM for elastic-plastic deformation based on incremental strain theory is used for the analysis of triangular pyramidal indentation. Only the outline of the proposed method is explained here because the general formulation and establishment of boundary conditions for the calculation are described in detail elsewhere (Murakami *et al.*, 1994). Based on the shape of the triangular pyramidal indenter and the deformation of specimen, conventional constant-strain tetrahedron elements are used. However, an appropriate meshing pattern of the elements must be selected in order to obtain an accurate solution. After trial and error the specimen to be indented is assumed to take the form of a hexagonal pyramid. The positional relationship between the triangular pyramidal indenter and the specimen to be indented is illustrated in Fig. 2 and the shape of the triangular pyramidal indenter is illustrated in Fig. 3. The symbol ϕ defines the apical angle and α the nominal angle between the face and the vertical axis. If the symmetry of the problem is taken into account, the calculation is conducted in the domain OABC under the assumption of a frictionless contact by a rigid triangular pyramid with $\phi = 115$ deg ($\alpha = 65$ deg), which is the value of the triangular pyramidal diamond indenter generally used in micro-hardness testing. Although FEM methods have been established for the calculation of three-dimensional elasto-plasticity, special consideration must be given to the treatment of the boundary conditions in order to calculate the triangular pyramidal indentation; it is necessary to set up the FEM program developed by ourselves. The characteristics of the proposed analytical method for treating the nodal points on the three boundaries is described in the following.

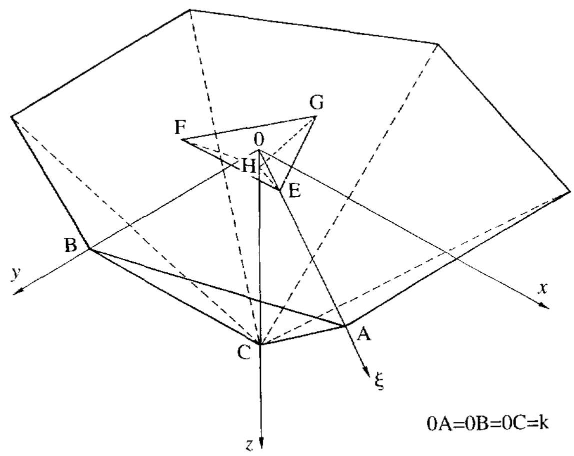

Fig. 2. Analytical model.

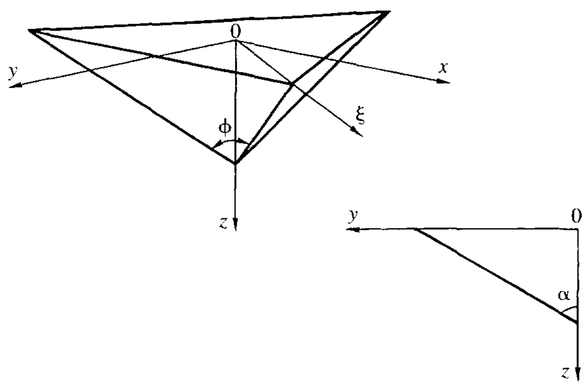

Fig. 3. Shape of triangular pyramidal indenter.

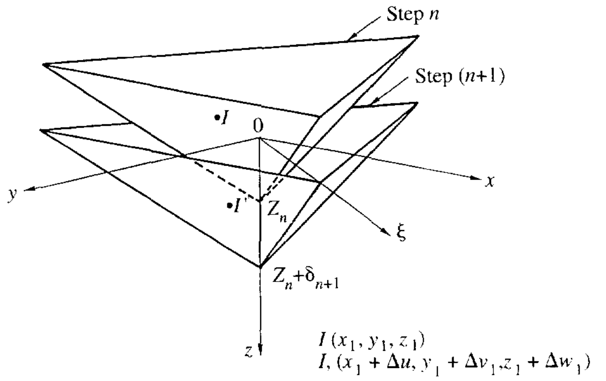

Fig. 4. Displacement boundary condition.

2.1. *The nodes of the boundary OAC*

In order to conduct the calculation based on incremental strain theory, we denote the incremental displacements of a nodal point in the x, y and z directions as Δu, Δv and Δw, and the incremental loads as ΔF_x, ΔF_y and ΔF_z, respectively.

We consider that a nodal point $I(x_I, y_I, z_I)$ is moved to a point $I'(x_I+\Delta u_I, y_I+\Delta v_I, z_I+\Delta w_I)$ by the indentation step from n to $n+1$. Then the corresponding nodal force in the normal direction is changed from F_I to $F_I+\Delta F_I$. When the nodal point lies on the boundary OAC, it is constructed against normal displacement and must satisfy the incremental displacement-boundary condition,

$$\Delta u_I - \gamma \Delta v_I = 0, \tag{1}$$

where γ is $\tan\theta$ with $\theta = \angle \mathrm{BOA} = \pi/3$. Since the nodal force on the boundary OAC acts in the normal direction, it must satisfy the incremental load-boundary conditions,

$$\gamma \Delta F_{Ix} + \Delta F_{Iy} = 0, \tag{2}$$

$$\Delta F_{Iz} = 0. \tag{3}$$

2.2. *The nodes in contact with the indentation surface*

The displacement of the triangular pyramidal indenter surfaces by the indentation step from n to $n+1$ is shown in Fig. 4. When the nodes are in contact with the indentation surface, but not on the ridge line HE (Fig. 2) of the indenter, the incremental displacement-boundary condition is given as

$$\Delta v_I + \beta(\Delta w_I - \delta_{n+1}) = 0, \tag{4}$$

where β is $\tan\alpha$ and δ_{n+1} is the incremental displacement of the rigid indenter in the z direction at step $n+1$. Because of the frictionless contact, only the normal traction acts on the contact surface. This leads to the incremental load-boundary condition at the contact surface;

$$\Delta F_{Ix} = 0, \tag{5}$$

$$\Delta F_{Iy} - \Delta F_{Iz}/\beta = 0. \tag{6}$$

2.3. *The nodes on the ridge line HE*

When the contact nodes lie on the ridge line HE (Fig. 2) of the indenter, they must satisfy the boundary conditions for both the contact surface and the OAC plane. That is, the relevant incremental nodal force components of the node I on the ridge line should be the sum of the reaction forces from these two planes. Thus combining eqns (2) and (3) with eqns (5) and (6) gives the incremental load boundary condition for the nodes on the ridge line of the triangular indenter as

$$\gamma \Delta F_{Ix} + \Delta F_{Iy} - \Delta F_{Iz}/\beta = 0. \tag{7}$$

2.4. *Composition of the stiffness matrix for the incremental loading process*

We next compose the FEM equations for the nodes of three particular boundaries. If we pay attention to the incremental loads and the incremental displacements for the nodes at the OAC plane which must satisfy the boundary conditions of eqns (1), (2) and (3), the FEM equations can be written as

$$\begin{bmatrix} \vdots & & \vdots & \vdots & \vdots & \\ \gamma k_{3I-2,1}+k_{3I-1,1} & \cdots & \gamma k_{3I-2,3I-2}+k_{3I-1,3I-2} & \gamma k_{3I-2,3I-1}+k_{3I-1,3I-1} & \gamma k_{3I-2,3I}+k_{3I-1,3I} & \cdots \\ 0 & 0 & 1.0 & -\gamma & 0 & 0 \\ k_{3I,1} & \cdots & k_{3I,3I-2} & k_{3I,3I-1} & k_{3I,3I} & \cdots \\ \vdots & & \vdots & \vdots & \vdots & \end{bmatrix} \begin{bmatrix} \vdots \\ \Delta u_I \\ \Delta v_I \\ \Delta w_I \\ \vdots \end{bmatrix} = \begin{bmatrix} \vdots \\ 0 \\ 0 \\ 0 \\ \vdots \end{bmatrix}, \tag{8}$$

where k denotes the incremental stiffness matrix components. For the nodes in contact with the indentation surface excluding the ridge line HE of the indenter, the boundary conditions of eqns (4), (5) and (6) must be satisfied, and then the FEM equations can be written as

$$\begin{bmatrix} \vdots & & \vdots & \vdots & \vdots & \\ k_{3I-2,1} & \cdots & k_{3I-2,3I-2} & k_{3I-2,3I-1} & k_{3I-2,3I} & \cdots \\ k_{3I-1,1}-k_{3I,1}/\beta & \cdots & k_{3I-1,3I-2}-k_{3I,3I-2}/\beta & k_{3I-1,3I-1}-k_{3I,3I-1}/\beta & k_{3I-1,3I}-k_{3I,3I}/\beta & \cdots \\ 0 & 0 & 0 & 1.0 & \beta & 0 \\ \vdots & & \vdots & \vdots & \vdots & \end{bmatrix} \begin{bmatrix} \vdots \\ \Delta u_I \\ \Delta v_I \\ \Delta w_I \\ \vdots \end{bmatrix} = \begin{bmatrix} \vdots \\ 0 \\ 0 \\ \beta\delta_{n+1} \\ \vdots \end{bmatrix}. \tag{9}$$

For the nodes on the ridge line HE of the indenter, the boundary conditions of eqns (1), (4) and (7) must be satisfied, resulting in:

$$\begin{bmatrix} & \vdots & \vdots & \vdots & \\ \cdots & \gamma k_{3I-2,3I-2}+k_{3I-1,3I-2}-k_{3I,3I-2}/\beta & \gamma k_{3I-2,3I-1}+k_{3I-1,3I-1}-k_{3I,3I-1}/\beta & \gamma k_{3I-2,3I}+k_{3I-1,3I}-k_{3I,3I}/\beta & \cdots \\ 0 & 1.0 & -\gamma & 0 & 0 \\ 0 & 0 & 1.0 & \beta & 0 \\ & \vdots & \vdots & \vdots & \end{bmatrix} \begin{bmatrix} \vdots \\ \Delta u_I \\ \Delta v_I \\ \Delta w_I \\ \vdots \end{bmatrix} = \begin{bmatrix} \vdots \\ 0 \\ 0 \\ \beta\delta_{n+1} \\ \vdots \end{bmatrix}. \tag{10}$$

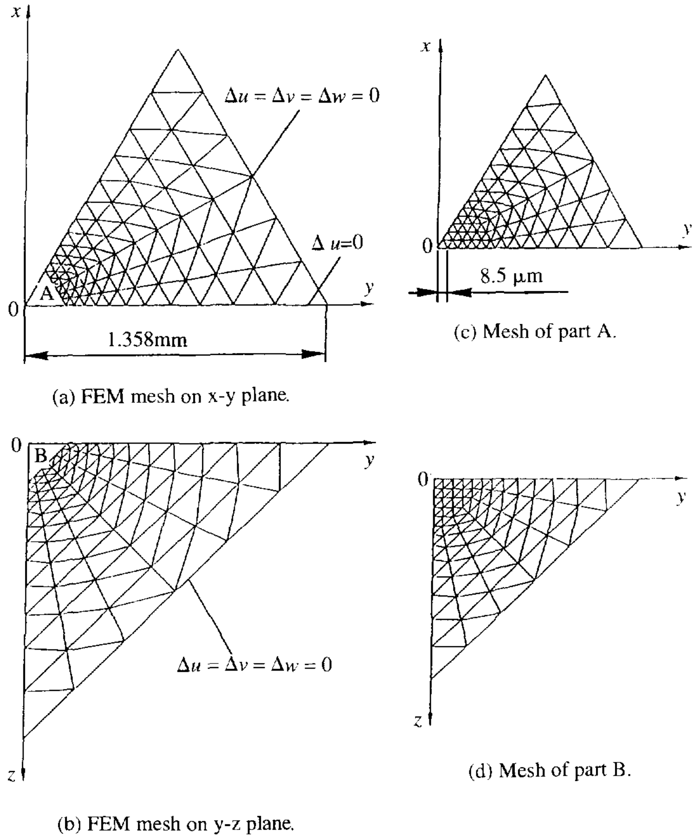

The length of the minimum side of
the minimum element = 8.5 μm.

Fig. 5. Finite element mesh. (a) FEM mesh on x-y plane. (b) FEM mesh on y-z plane. (c) Mesh of part A. (d) Mesh of part B.

2.5. *FEM mesh, the boundary condition of specimen and test materials*

The mesh pattern of the analyzed domain OABC, shown in Fig. 2, is illustrated in Fig. 5. The total numbers of nodes and elements are 588 and 2160, respectively. The length of outer boundary OA(= OB = OC) is 1.358 mm. The closest spacing of nodes is immediately beneath the contact surface and the dimension of the corresponding elements is 8.5 μm. To satisfy the symmetry condition, the node on the boundary OBC, which is constrained against the nominal displacement or the incremental displacement in the x direction, is $\Delta u = 0$. The nodes of the boundary ABC are fixed as $\Delta u = \Delta v = \Delta w = 0$. The validity of this boundary condition was checked in a previous paper (Murakami and Matsuda, 1994).

A three-dimensional finite element method based on the strain incremental plastic theory Prandtl-Reuss equation (Zienkiewicz, 1971) is used for the numerical analysis of the triangular pyramidal indentation. Stress-strain curves of 0.46% carbon steel and 70/30 brass in tensile tests are shown in Fig. 6. The true stress-logarithmic strain curves of these two materials are used for the analysis of triangular pyramidal indentation. The yield stress of 0.46% carbon steel is 337 MPa and that of 70/30 brass is 81.7 MPa. Considering the results of the Vickers hardness analysis by the FEM in the previous paper (Murakami and Matsuda, 1994), the isotropic hardening rule is used for this FEM analysis. The elements which satisfy the Mises yield criterion within $\pm 1\%$ error are regarded as yielded elements. The deformed shape of the specimen is determined by adding stepwise incremental displacements to the previous coordinates of nodes. Because the number of calculation steps is 268 in 0.46% carbon steel and 770 in 70/30 brass for the indentation (loading) process, the deformation per one step can be considered sufficiently small for use of incremental strain theory. The maximum indentation load, P_{max} for the microhardness test is 9.8 N (1 kgf).

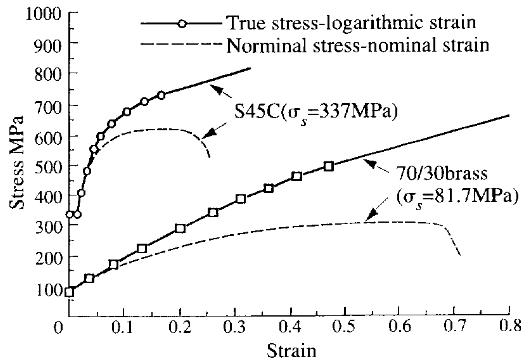

Fig. 6. Stress strain curve of 0.46%C steel and 70/30 brass.

3. RESULTS AND DISCUSSION

3.1. *The shape of indentation*

The micrograph of the triangular pyramidal diamond indentation for 0.46% carbon steel after removal of the load, $P_{max} = 9.8$ N (1 kgf), is shown in Fig. 7. The hardness with triangular pyramidal indenter is defined by the applied load divided by the surface area of a triangular diamond pyramid as the Vickers hardness. Since the shape of the triangular pyramidal indent projected onto the specimen surface plane is an equilateral triangle, as shown in Fig. 7, the hardness is calculated by the height of the equilateral triangle, d.

The deformed shape of elements in the vicinity of the origin for $P = P_{max} = 9.8$ N (1 kgf) in the FEM calculation is shown in Fig. 8, where the $\xi - y$ plane is viewed from the direction inclined to the horizon by 15 deg and rotated counterclockwise around the z-axis by 30 deg. In this case the eleven nodal points are in contact with indenter and denoted by the symbol ●.

The profile of the indentation on the y-axis for 0.46% carbon steel and 70/30 brass after unloading are shown in Fig. 9. The definition of the indentation size d in the FEM analysis is in a sense arbitrary because each node of elements are connected by straight lines during deformation. In this study, the edge of the indentation was defined as shown in Fig. 9 by the intersection of two lines: one is the line extended from the center of indentation and the other is the line extended from outside of indentation. Thus, the indentation size is $d = 0.096$ mm ($d/3 = 0.032$ mm) for 0.46% carbon steel and $d = 0.159$ mm ($d/3 = 0.053$ mm) for 70/30 brass.

3.2. *Comparison of numerical results with experimental results*

The hardness test was conducted by a commercial microhardness tester which was equipped with the triangular diamond pyramidal indenter whose apical angles was 115 deg.

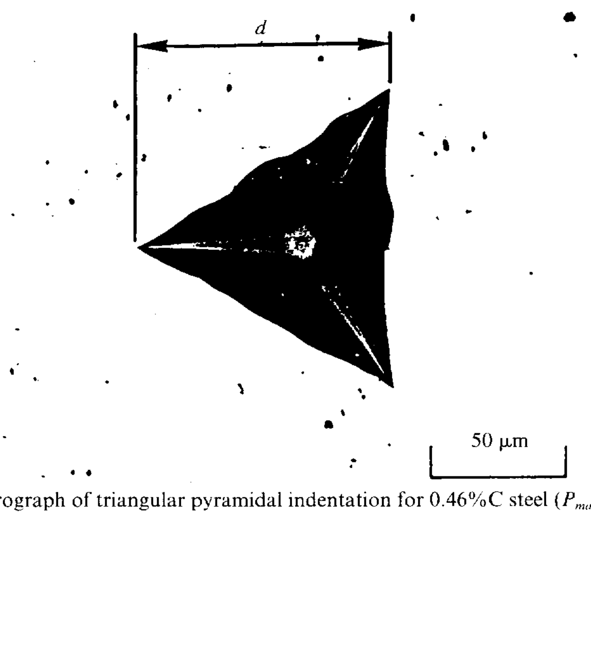

Fig. 7. Micrograph of triangular pyramidal indentation for 0.46%C steel ($P_{max} = 9.8$ N).

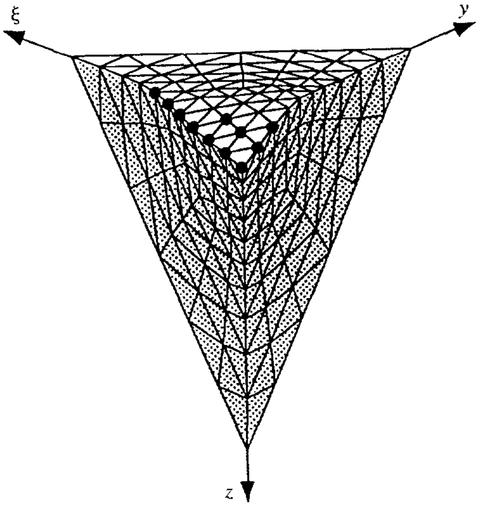

Fig. 8. Deformation of elements in the vicinity of the origin at $P = P_{max} = 9.8$ N for 0.46%C steel.

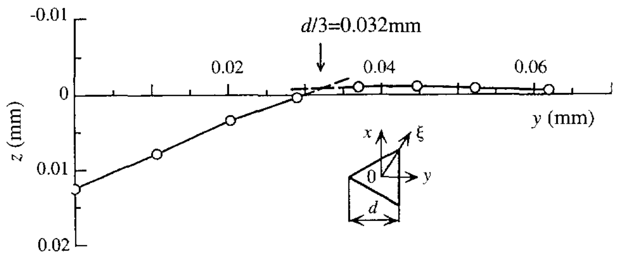

(a) 0.46%C steel (P_{max}=9.8N).

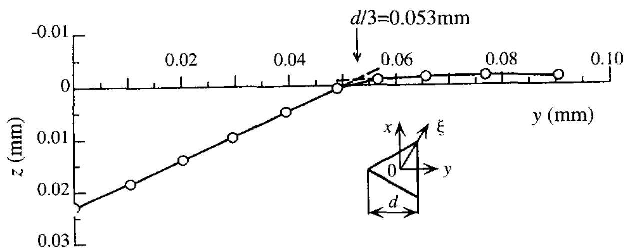

(b) 70/30 brass (P_{max}=9.8N).

Fig. 9. Shape of indentation on y-axis after unloading. (a) 0.46%C steel ($P_{max} = 9.8$ N). (b) 70/30 brass ($P_{max} = 9.8$ N).

The testing was performed using a peak load $P_{max} = 9.8$ N (1 kgf) for 30 seconds. The specimens were annealed after machining and subsequently, polished with emery paper and powder before testing. Three measurements of microhardness in one specimen were averaged. Table 1 compares the numerical and experimental results for 0.46% carbon steel and 70/30 brass. The scatter of indentation sizes of three tests was 1.2% for 0.46% carbon steel and 1.6% for 70/30 brass. The difference of the indentation sizes between numerical and experimental result is smaller than the scatter of the experimental results. Thus, the analytical method developed in this study may be considered accurate enough and useful for the analysis of triangular pyramidal indentations.

3.3. *The load-penetration depth curve and the mechanical properties*

Because the indentations made by a conical or pyramidal indenter are geometrically similar regardless of their size (except at very low loads), the mean pressure at the indentation, i.e. the hardness, should be independent of load. The load-penetration depth curve

Table 1. Comparison of numerical and experimental results for 0.46%C steel and 70/30 brass.

	P_{max}	d (mm)	δ (mm)	δ/d	H_{T115} (GPa)
S45C					
Experiment	9.8 N (1 kgf)	0.097	0.010	0.103	1.634
Calculation	9.8 N (1 kgf)	0.096	0.012	0.125	1.669
70/30 brass					
Experiment	9.8 N (1 kgf)	0.161	0.024	0.149	0.593
Calculation	9.8 N (1 kgf)	0.159	0.023	0.145	0.608

obtained from such an indenter contains much information related to the mechanical properties of the materials. In this section the load-penetration depth curve is analyzed with relation to the geometrical similarity and the mechanical properties (Cook and Pharr, 1994).

The load P and penetration depth δ curves calculated by the developed method are shown in Fig. 10. The number of the nodes in contact with the triangular pyramidal indenter at the maximum load is 11 for 0.46% carbon steel (shown in Fig. 8 by the symbol ●) and 21 for 70/30 brass. The meshing of the elements and the applied load are selected by a preliminary analysis which proved the reliability of the solution only for a sufficient number of contact nodes. The loading process is essentially different from the unloading process in Fig. 10. The curves of the loading process have several kinked points which are caused by the contact of the nodal points on the ξ-axis with the ridge line of the indenter. On the other hand, the unloading curves are smooth. Because the curves of the loading process in the elastic analysis of triangular pyramidal indentation did not have such clear kinked points, it is thought that the kinked points in the loading process are associated with an increase in the number of nodal points in contact with the indenter and the subsequent extension of the plastic zone.

Figure 11 replots the data of Fig. 10 using logarithmic axes. Figure 11(a) represents the curves of the loading process and Fig. 11(b) the curves of the unloading one where δ_f is the final remnant plastic displacement. The lines in Fig. 11 indicate the equations calculated by the least squares method using the data near the maximum load. In the loading process the slope of the lines is slightly smaller than 2.0 which is a pure quadratic relationship between load and penetration depth. On the other hand the slope of initial unloading portion is approximately 2.0. In order to interpret the relation between load and penetration depth which cannot be a pure quadratic one in micro Vickers hardness region, Bernhardt (Bernhardt, 1941) proposed the following eqn (11).

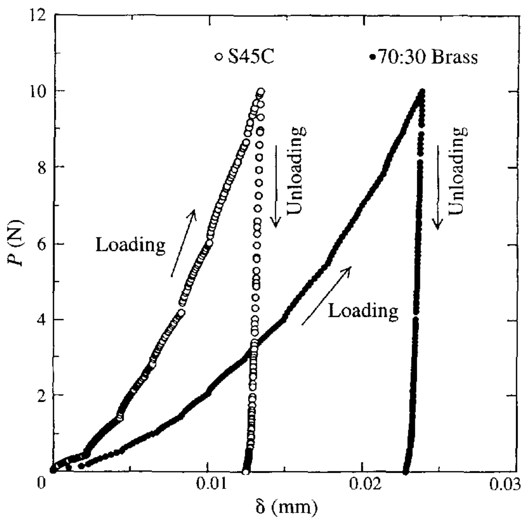

Fig. 10. Relationship between load P and penetration depth δ.

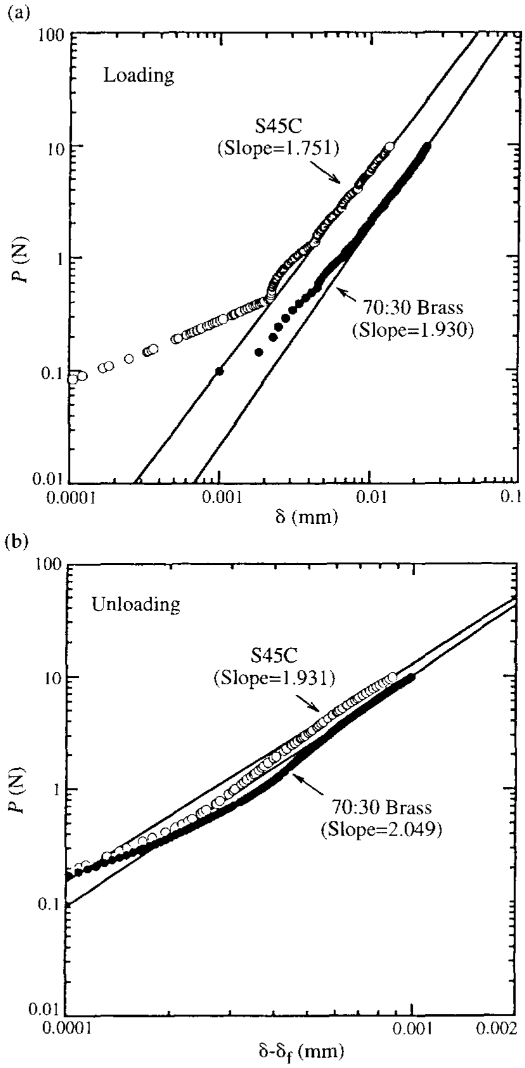

Fig. 11. Relationship between P and δ plotted using logarithmic coordinates. (a) Loading process. (b) Unloading process.

$$P = A\delta + B\delta^2. \tag{11}$$

Bernhardt pointed out that the linear term in eqn (11) arises, when additional attributes of certain surfaces are taken into consideration. Maschke and Seifert (Maschke and Seifert, 1982) derived generalizations of Bernhardt's formula for micro-indentation tests which make allowance to surface-layers with non-vanishing thickness. In this study the analytical model is used as homogeneous materials without surface-layers.

Figure 12 shows the P/δ and δ relationship replotted from Fig. 10. The lines in Fig. 11 indicate the equations calculated by the least squares method using the data near the maximum load. It seems that the lines in Fig. 11 have the intercept at the vertical axis which gives the linear term in eqn (11) and the value of the intercept depends on the materials. According to the elastic analysis of the triangular pyramidal indentation the value of the intercept is considered to be zero. Even in plastic analysis, if the shape of indentation is always geometrically similar regardless the values of load, the value of the intercept should be zero. However, in combined condition of elastic and plastic deformation, the yielding occurs uncontinuously in certain critical zone with elastic stress gradient. Thus, it is thought that the value of the intercept is correlated with the size effect in yielding phenomenon.

An evaluation of the mechanical properties from the load penetration depth curves in the ultra-low load hardness test has been attempted by several researchers. The two most

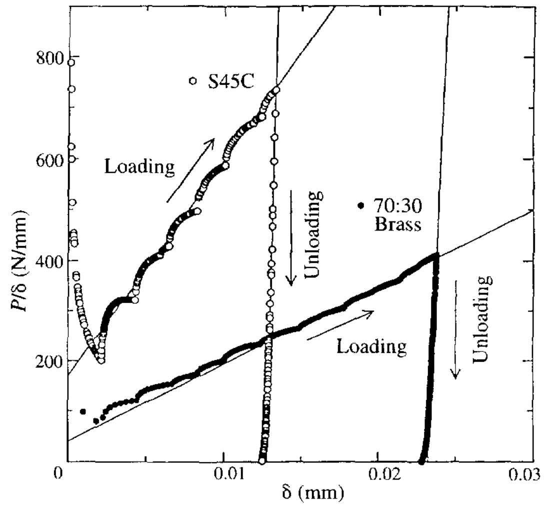

Fig. 12. Relationship between P/δ and δ.

frequently measured mechanical properties are the hardness from the loading curve and the elastic modulus from the unloading curve (Inamura *et al.*, 1990; Söderlund and Rowcliffe, 1994). Also in the present calculated results it is ensured that the slope of the loading portion in Fig. 12 can be correlated with the hardness, and the slope of the unloading portion with Young's modulus.

3.4. *The extension of the plastic zone*

The extension of the plastic zone in the specimen at several loading steps is shown in Fig. 13. For 0.46% carbon steel at the load $P = P_{max}$, the extension of the plastic zone on the specimen surface is $1.3 \sim 1.5$ times larger than the indentation size d, and the periphery of the plastic zone is slightly expanded toward the ξ-axis direction, the direction of the ridge line of the indenter. The depth of the plastic zone is approximately 1.5 times the indentation size d and 12 times the indentation depth. On the other hand for 70/30 brass at the load $P = P_{max}$, the extension of the plastic zone on the specimen surface is 1.8 times the indentation size d, and the periphery of the plastic zone is nearly circular. The depth of the plastic zone is approximately 1.8 times the indentation size d and 12 times the indentation depth. Such numerical results will be useful in estimating the mechanical properties of materials used in very thin layers by the ultra-low load hardness test. As consideration of these numerical results requires a determination of the depth of the indentation to be made to the thin layer compared with the thickness, because the experimental results are influenced by material thickness in the ultra-low load hardness test. These problems must be discussed in more detail in future research.

3.5. *The stress distribution in the vicinity of the ξ-axis*

Figure 14 shows the stress distribution in the vicinity of the ξ-axis for $P = P_{max}$. There are no tensile stresses in the vicinity of the indenter, and the profiles of the stress distribution for 0.46% carbon steel and 70/30 brass are similar. The stress peaks exist at the position of $\xi/(2d/3) = 0.7$ from the center of contact surface.

Figure 15 shows the distribution of residual stresses in the vicinity of the ξ-axis after unloading. All of the residual stresses in the vicinity of the ξ-axis for both the materials are compressive. In the results of the analysis of the Vickers hardness by Murakami and Matsuda, there is large tensile residual stress in the vicinity of the indentation for 0.46% carbon steel and 70/30 brass after unloading, and they pointed out the effect of the tensile residual stress on the initiation of indentation cracks in ceramics (Murakami and Matsuda, 1994). In the hardness test of the triangular diamond pyramidal indenter for ceramics, the authors have confirmed that the indentation cracks initiate on the extended line of the ridge of the indentation after unloading as well as the Vickers hardness test. Comparing the

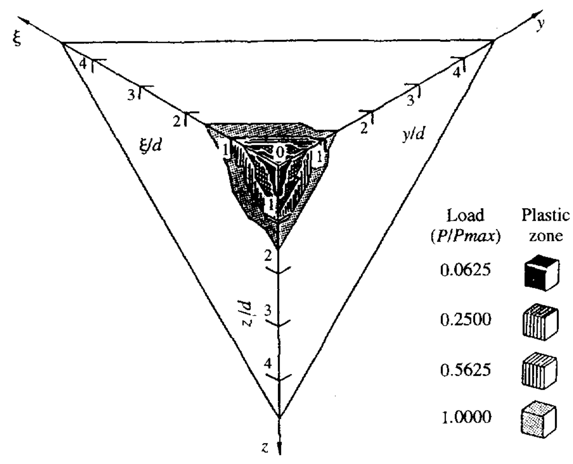

(a) 0.46%C steel.

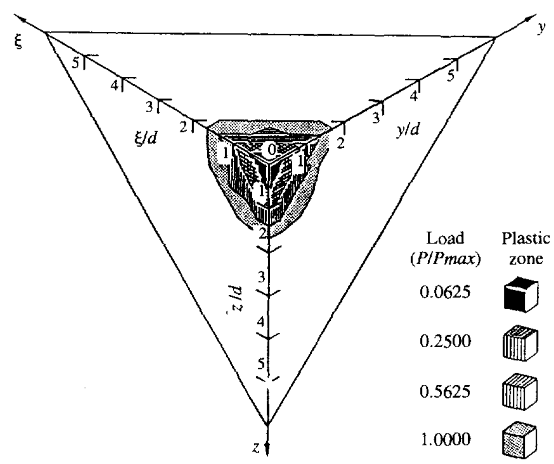

(b) 70/30 brass.

Fig. 13. Extension of plastic zone. (a) 0.46%C steel. (b) 70/30 brass.

profile of the distribution of residual stresses for 0.46% carbon steel with that for 70/30 brass in Fig. 15, it is found that the residual stresses approach the positive (tension) for 70/30 brass more than 0.46% carbon steel at $\xi/(2d/3) = 1$ and the magnitude of the residual stresses is dependent on the materials used. Since the exact stress-strain curves, i.e. constitutive equations of ceramics, are not known, it is difficult to determine the exact distribution of the residual stresses.

4. CONCLUSION

(1) A particular formulation of the three-dimensional finite-element method is established for the elastic-plastic analysis of a triangular pyramidal indentation.

(2) Triangular pyramidal indentations on 0.46% carbon steel and 70/30 brass are analyzed by the developed method using the tensile stress-strain curves. The calculated results are in good agreement with the experimental results.

(3) The curve of the calculated load-penetration depth is analyzed with relation to the geometrical similarity. The loading curve is slightly out of a pure quadratic relationship between load and penetration depth. It is thought that the deviation from a pure quadratic relation is correlated with the size effect in yielding phenomenon.

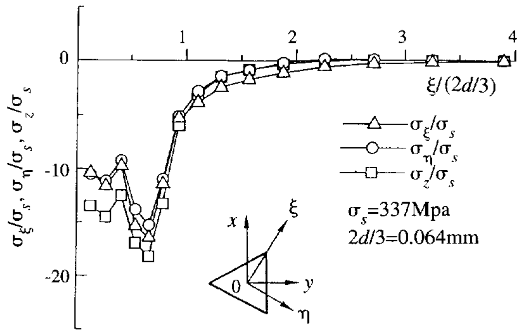

(a) 0.46%C steel.

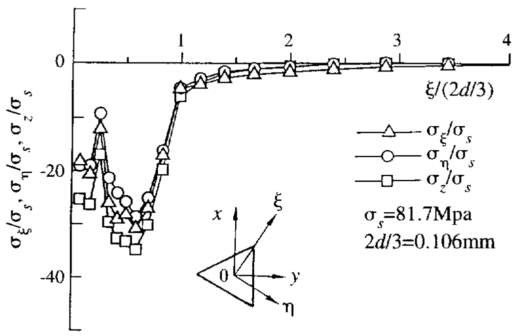

(b) 70/30 brass.

Fig. 14. Stress distribution in the vicinity of ξ-axis ($P = P_{max}$). (a) 0.46%C steel. (b) 70/30 brass.

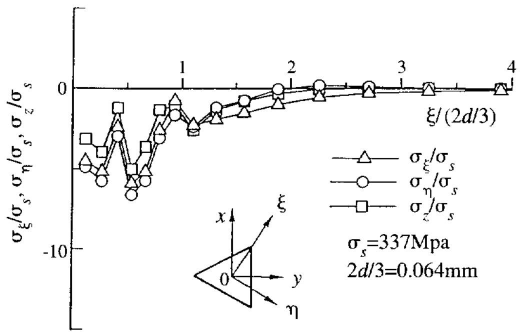

(a) 0.46%C steel.

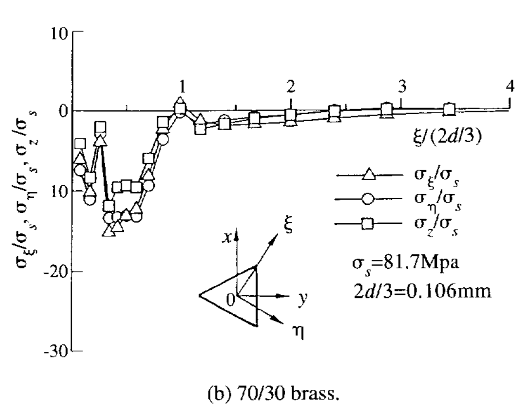

(b) 70/30 brass.

Fig. 15. Residual stress distribution in the vicinity of ξ-axis. (a) 0.46%C steel. (b) 70/30 brass.

Acknowledgements—The authors thank Prof. Kohichi Tanaka, Nagaoka University of Technology, for the useful discussion on this paper. This study was financially supported by the respective Grant-in-Aids No. 04402022, for Science Research from the Ministry of Education of Japan.

REFERENCES

Barber, J. R. and Billings, D. A. (1990) An approximate solution for the contact area and elastic compliance of a smooth punch of arbitrary shape. *International Journal of Mechanical Sciences* **32,** 991–997.

Berkovich, E. S. (1951) Three-faceted diamond pyramid for micro-hardness testing. *International Diamond Review* **11,** 129–132.

Bernhardt, E. O. (1941) Über die Mikrohärte der Feststoffe im Grenzbereich des Kick'schen Ähnlichkeitssatzes. *Zeitschrift für Metallkunde* **33,** 135–144.

Bilodeau, G. G. (1992) Regular pyramid punch problem. *Journal of Applied Mechanics* **59,** 519–523.

Cook, R. F. and Pharr, G. M. (1994) Indentation load-displacement behaviour during conventional hardness testing. *Journal of Hard Materials* **5,** 179–190.

Doerner, M. F. and Nix, W. D. J. (1986) A method for interpreting the data from depth-sensing indentation instruments. *Material Research* **1,** 601–609.

Inamura, M. and Suzuki, T. (1990) Evaluation of materials strength by ultra-micro-indentation. *SEISAN KENKYU* **42,** 257–250 (in Japanese).

Kaneko, R. (1991) Present and future of magnetic disk storages. *Japanese Society of Tribologists* **36,** 587–591 (in Japanese).

Larsson, P.-L., Giannakopoulos, A. E., Söderlund E., Rowcliffe, D. J. and Vestergaard, R. (1996) Analysis of Berkobich indentation. *International Journal of Solids and Structures* **33,** 221–248.

Maschke, H. and Seifert, W. (1982) Generalization of Bernhardt's formula for micro-indentation tests. *ExperimentelleTechnikderPhysik* **30,** 11–18.

Murakami, Y., Tanaka, K., Itokazu, M. and Shimamoto, A. (1994) Elastic analysis of triangular pyramidal indentation by the finite-element method and its application to nano-indentation measurement of glasses. *Philosophical Magazine A* **69,** 1131–1153.

Murakami, Y. and Matsuda, K. (1994) Analysis of Vickers hardness by the finite element method. *Journal of Applied Mechanics* **61,** 822–828.

Ohmae, N. and Tagawa, M. (1992) Microtribology. *Journal of Japanese Society Tribologists* **37,** 10–16 (in Japanese).

Olaf, J. M. and Scheer, C. (1993) Finite element analysis of indentation experiments in surfaces and surface coated materials. *Computational Materials Science* **1,** 276–282.

Page, T. F., Oliver, W. C. and McHargue, C. J. (1992) The deformation of ceramic crystals subjected to very low load (nano) indentations. *Journal of Materials Research* **7,** 450–473.

Pethica, J. B., Hutchings, R. and Oliver, W. C. (1983) Hardness measurement at penetration depths as small as 20 nm. *Philosophical Magazine A* **48,** 593–606.

Shimamoto, A., Nishimori, K., Tanaka, K., Sugiyama, T. and Shinohara, T. (1993) Surface spectroscopy and tribology of overcoat carbon film prepared by spattering in a methane and argon mixed gas atmosphere. *Advances in Infinite Storage Systems* **5,** 259–272.

Söderlund E. and Rowcliffe, D. J. (1994) Analysis of penetration curves produced by depth-sensing indentation systems. *Journal of Hard Materials* **5,** 149–177.

Tsukamoto, Y., Yamaguchi, H. and Yanagisawa, M. (1987) Mechanical properties of thin films: measurements of ultramicroindentation hardness, Young's modulus and internal stress. *Thin Solid Films* **154,** 171–181.

Yanagisawa, M. and Motomura, Y. (1987) An ultramicro indentation hardness tester and its application to thin films. *Lubrication Engineering* **43,** 52–56.

Yanagisawa, M. (1991) Tribology of sputtered magnetic recording disks. *Journal of Japanese Society Tribologists* **36,** 265–270 (in Japanese).

Zienkiewiez, O. C. (1971) *The Finite Element Method in Engineering Science*. McGraw-Hill, London.